Positional information encoded in the dynamic differences between neighbouring oscillators during vertebrate segmentation.

Marcelo Boareto[1,2], Tomas Tomka[1] and Dagmar Iber[1,2,*]

Affiliations

[1] *Department of Biosystems Science and Engineering (D-BSSE), ETH Zurich, Mattenstrasse 26, 4058 Basel, Switzerland*

[2] *Swiss Institute of Bioinformatics, Mattenstrasse 26, 4058 Basel, Switzerland.*

*Correspondence to: dagmar.iber@bsse.ethz.ch

Abstract

How cells track their position during the segmentation of the vertebrate body remains elusive. For decades, this process has been interpreted according to the clock-and-wavefront model, where molecular oscillators set the frequency of somite formation while the positional information is encoded in signaling gradients. Recent experiments using *ex vivo* explants challenge this interpretation, suggesting that positional information is encoded in the properties of the oscillators. Here, we propose that positional information is encoded in the difference in levels of neighboring oscillators. The differences gradually increase because both the oscillator amplitude and the period increase with time. When this difference exceeds a certain threshold, the segmentation program starts. Using this framework, we quantitatively fit experimental data from *in vivo* and *ex vivo* mouse segmentation, and propose mechanisms of somite scaling. Our results suggest a novel mechanism of spatial pattern formation based on the local interactions between dynamic molecular oscillators.

Introduction

Pattern formation during embryonic development requires that the cells assess their spatial position. One useful conceptual framework to understand this process is to assume that each cell has a positional value that relates to its position in the coordinate system. The cells then use this positional information to coordinate their differentiation process (Wolpert, 1969). Based on this conceptual framework, Cooke and Zeeman proposed a model to explain the sequential and periodic formation of the somites in the vertebrate embryo. In their model, the positional information of the cells is given by a signaling wavefront, while a clock sets the frequency of somite formation (Cooke and Zeeman, 1976).

The ‘clock-and-wavefront’ model guided much of the experimental work done in the subsequent decades. It has been shown that the rhythm of segmentation is accompanied by travelling waves of gene expression, which sweep from the tail bud to the anterior end of the presomitic mesoderm (PSM) (Masamizu et al, 2006). These waves emerge from the oscillatory expression of ‘clock’ genes involved in the Notch pathway, such as *Lfng* and *Hes* (McGrew et al 1998; Palmeirim et al., 1997; Forsberg et al, 1998; Dequeant et al., 2006; Niwa et al., 2007). In the tail bud region, where the PSM cells are generated, *Fgf8* and *Wnt3* are produced and as the cells cross the PSM their mRNA levels decrease due to degradation, creating a gradient by inheritance (Dubrulle and Pourquié 2004; Aulehla et al, 2003). Perturbations on Wnt and Fgf gradients have been shown to affect somite formation (Dubrulle et al, 2001; Sawada et al, 2001; Naiche et al 2011), therefore suggesting that these signaling gradients could in principle encode the wavefront of somite formation.

Recently, experiments of *ex vivo* explants have challenged the ‘clock-and-wavefront’ view and favored an interpretation where the wavefront is implicit in the dynamics of the clock (Lauschke et al, 2013). In these experiments, tail bud tissue is explanted and forms a monolayer PSM (mPSM) with concentric travelling waves sweeping from the center of a dish to its periphery. Interestingly, after growth stops, segments begin to form, and the size of the segments scales with the size of the mPSM (Lauschke et al 2013). The formation of these segments in the absence of growth cannot be easily explained with the ‘clock-and-wavefront’ model as it would require long-range mechanisms that sense the mPSM length. An alternative model was proposed where the wavefront is defined via the relative phase of a cellular oscillator compared to the tail bud oscillation (Lauschke et al., 2013). Since then, mechanistic networks that can compute such a relative phase of oscillation have been investigated (Beaupeux and François, 2016). A possible explanation includes two signaling oscillators in each cell and the phase shift between these oscillators would determine segmentation (Lauschke et al., 2013; Beaupeux and François, 2016, Sonnen et al, 2018). However, how these oscillators would control *in vivo* segmentation remains unclear.

The *Hes/her* genes are key targets of the Notch signaling pathway and form the central components of the cellular oscillators that control somite formation (Takke and Campos-Ortega, 1999; Bessho et al, 2001; Kageyama et al, 2007). In various species, these genes have been shown to oscillate due to a delayed autoinhibition, although there is a substantial variability in the gene network (Krol et al, 2011; Hirata et al 2002; Oates and Ho 2002; Lewis 2003). In many species, the period of Hes/her oscillations increases in time as the cells move from the posterior to the anterior part of the PSM (Delaune et al, 2012; Shih et al, 2015, Gomez et al, 2008, Tsiaris and Aulehla, 2016). The same is true for the amplitude of the oscillators, as quantified in zebrafish (Delaune et al, 2012; Shih et al, 2015), and indirectly shown in mouse (Lauschke et al, 2013, Tsiaris and Aulehla, 2016). Interestingly, this temporal increase in period and amplitude correlates with the temporal decrease of Fgf and Wnt

signaling due to mRNA degradation. Moreover, Fgf and Wnt signaling have been shown to modulate the properties of Hes/her oscillators (Niwa et al, 2007; Kawamura et al, 2005; Wiedermann et al, 2015). This suggests a possible link between the gradient of Fgf/Wnt signaling and the properties of Hes/her oscillators, where the temporal decay in Fgf/Wnt signaling due to mRNA degradation leads to a temporal increase in the period and amplitude of Hes/her oscillations.

A set of neighboring oscillators with slight differences in period and amplitude are known to lead to travelling waves. This can be visualized in a pendulum wave experiment, where a set of pendulums with gradually increased lengths that start from the same initial condition display a travelling wave (Berg, 1991; Flaten and Parendo, 2001). This is a result of the temporal accumulation of differences in the levels of neighboring oscillators. Inspired by this mechanism, we propose that positional information during somite formation is encoded by the differential levels of neighboring Hes/her oscillators. When the cells are generated in the tail bud region, they start with the same initial condition and Hes/her oscillations are synchronized with their neighbors. As the cells leave the tail bud region and cross the PSM, a temporal increase in the period and amplitude of Hes/her oscillations leads to a gradual increase in the difference of Hes/her levels in neighboring cells. We propose that the differential levels between neighboring oscillators represent the positional value that encodes the information required to start the segmentation program. In order to explore this mechanism, we first develop a theoretical framework. We then show that our model quantitatively fits *in vivo* mouse segmentation from wild type and growth-perturbed embryos, captures temperature compensation in somite size and predicts a delayed scaling between somite size and PSM length. We further use data from different species to suggest possible developmental mechanisms of somite size control. Lastly, we quantitatively fit data from mouse *ex vivo* explants, showing that the proposed mechanism can in principle explain data from both *in vivo* and *ex vivo* mouse segmentation.

Results

Theoretical framework

In our framework, we consider that each cell expresses an oscillatory protein *u* that represents a member of the Hes/her family. For simplicity, we represent the levels of *u* by a sine function:

$$u = A(x,t)\sin\phi(x,t), \tag{1}$$

where the amplitude *A* and the phase ϕ depend on the position of the cell *x* and the time *t*.

After leaving the tail bud region, the amplitude and period of the oscillations increase over time in the PSM cells (Delaune et al, 2012; Shih et al, 2015). We assume that the increase in the period and amplitude is given by the temporal decrease of Fgf/Wnt signal due to the gradient by inheritance. For convenience, we assume that the increase in the amplitude (A) and period (T) can be mathematically represented by exponential functions:

$$A = A_0 e^{\frac{\Delta t}{\alpha}} \tag{2}$$

$$T = T_0 e^{\frac{\Delta t}{\beta}} \tag{3}$$

where A_0 and T_0 are the amplitude and period at the tail bud region, respectively, and α and β are the characteristic time scale of amplitude and period gradients, respectively. Note that the period and, consequently, the frequency are dependent on the amount of time cell has spent in the tissue. This is represented by $\Delta t = t - t_0$, where $t_0 = t_0(x)$ represents the moment the cell in position x is incorporated into the PSM (Figure 1). We consider that each cell has a fixed position x, while the tail bud moves in the direction of increasing x (Figure 1). We further define the phase ϕ of the cellular oscillator by using the following relationship:

$$\omega = \frac{d\phi}{dt} \tag{4}$$

which results in:

$$\phi = (\omega_0 - \omega)\,\beta + \phi_0, \tag{5}$$

where ω is the frequency of oscillation and $\phi_0 = \omega_0\, t_0$ represents the initial phase of the cell with ω_0 being the frequency of the oscillator at the tail bud.

The slight difference in period and amplitude between neighboring cells leads to the temporal accumulation of differences in their expression levels. We propose that segmentation occurs when these differences reach a certain threshold (θ). This can be represented mathematically as:

$$\frac{\partial u}{\partial x} = \theta. \tag{6}$$

The derivative of u can be written as:

$$\frac{\partial u}{\partial x} = \frac{\partial u}{\partial \phi}\frac{\partial \phi}{\partial x} + \frac{\partial u}{\partial A}\frac{\partial A}{\partial x}, \tag{7}$$

which leads to:

$$\frac{\partial u}{\partial x} = A\cos\phi\frac{\partial\phi}{\partial x} + \sin\phi\frac{\partial A}{\partial x}. \tag{8}$$

By calculating the spatial derivative of *A* and φ, we have:

$$A\left((\omega_0 - \omega)\frac{\partial t_0}{\partial x}\cos\phi - \frac{1}{\alpha}\frac{\partial t_0}{\partial x}\sin\phi\right) = \theta, \tag{9}$$

where $\frac{\partial t_0}{\partial x}$ represents the rate at which the cells are being incorporated to the tail bud. It is associated to the tail bud growth rate by the following relationship:

$$\frac{\partial t_0}{\partial x} = \frac{1}{g_{t0}} \tag{10}$$

where g_{t0} is the tail bud growth rate at the time $t=t_0$. From Eq. 9, we then obtain:

$$\frac{A}{g_{t0}}\left((\omega_0 - \omega)\cos\phi - \frac{1}{\alpha}\sin\phi\right) = \theta. \tag{11}$$

Using the previous equation, we can infer the position of segmentation. Note that if we assume that A_0 is constant during the segmentation process, this parameter can be incorporated into the threshold θ. Therefore, our model has only 5 parameters: the characteristic time scale of the amplitude gradient (α), the characteristic time scale of the period gradient (β), the tail bud growth rate (g_{t0}), the oscillation period at the tail bud (T_0) and the normalized threshold (θ/A_0). Note that the segmentation mechanism is dependent on the tail bud growth rate at the time the cells are in the tail bud region (g_{t0}). Consequently, after the cells leave the tail bud, all parameters are defined and only Δt changes. This leads to a timer mechanism of somite formation, independent of any spatial input.

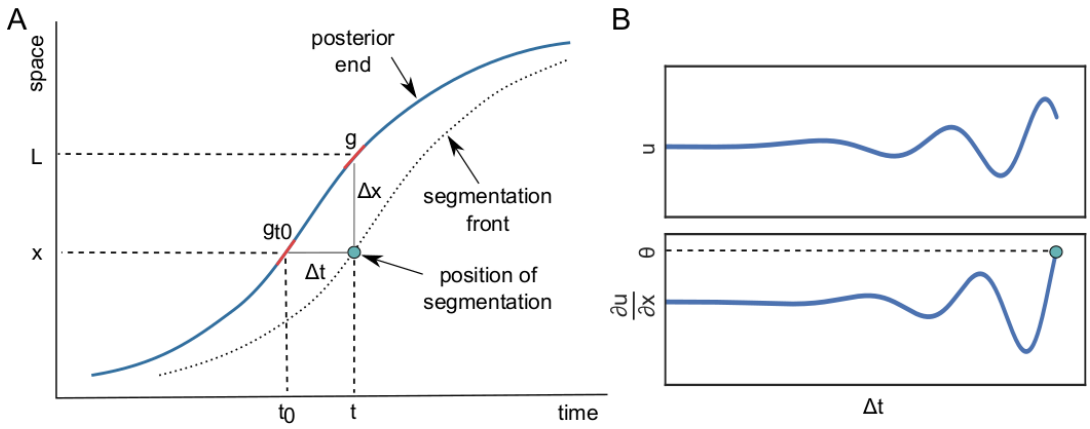

Figure 1. Schematic representation of segmentation process. *A) Blue curve represents the position of the posterior end in time, the green dot represents the position of segmentation where du/dx=θ. Δt=t-t_0 represents the amount of time since the cell at position x was incorporated to the tissue and Δx=L-x is the distance of the cell x to the posterior end at the time t. The tail bud growth rates g_{t0} and g represent the growth rate at the tail bud at the time t_0 and t, respectively. Note that $t_0 = t_0(x)$ such that $\frac{dt_0}{dx} = \frac{1}{g_{t0}}$. B) The amplitude and period of u increases over time, leading to an increase of du/dx until reaching a threshold θ at which segmentation occurs.*

Disturbed growth affects signaling gradients.

The segmentation of the vertebrate body is a highly dynamic process. The axial growth rate, the somite size, and the PSM length have been shown to vary broadly during embryonic development and are disturbed in animals that suffered drastic size reduction due to treatment with DNA-synthesis inhibitor Mitomycin C (MMC) (Tam 1981). During mouse somitogenesis, the axial growth rate presents a hump-shaped curve, an initial increase followed by a consecutive decrease (Tam 1981, Figure S1). As a consequence of such growth profile, the axial length increases in a sigmoid-like fashion during development (Tam 1981, Figure S1). Interestingly, although growth-perturbed (MMC-treated) embryos are significantly smaller than wild type (WT) at early stages, these embryos show compensatory growth, resulting in an embryo with normal final size (Tam 1981, Figure S1). Such compensatory growth, however, leads to a disturbed somitogenesis where both the PSM length and somite size are smaller compared to WT embryos (Tam 1981, Figure S2).

Using published experimental data from WT and MMC-treated embryos (Tam 1981), we tested if our model is able to correctly reproduce somite size and PSM length at different embryonic stages. For simplicity, we decided to keep all parameters fixed during the segmentation process, except the tail bud growth rate, which is highly dynamic and was inferred from experimental data (Tam 1981, Figures 2A,B and S1). However, we observed that segmentation period is also dynamic during mouse somitogenesis (Tam 1981, Figure

S3), suggesting that the period of the oscillators changes during this process. One of the key assumptions of our model is that the period and amplitude of the oscillators are dependent on the levels of Fgf/Wnt signal. In this case, we would expect the levels of Fgf/Wnt signal to be dynamic during the segmentation process. Since recent evidences have linked the levels of Fgf/Wnt to the proliferation rate of PSM cells (Amin et al, 2016), we assumed that the levels of these gradients are proportional to the tail bud growth rate. In this case, the amplitude and period of the oscillations at the tail bud can be considered as a function of the tail bud growth rate, such as:

$$A_0 = A'_0 e^{-\frac{g_{t0}}{\gamma}} \tag{12}$$

$$T_0 = T'_0 e^{-\frac{g_{t0}}{\gamma}}, \tag{13}$$

where g_{t0} is the growth rate when the cell is at the tail bud (at $t = t_0$), and γ is a constant. We observed that the inclusion of the parameter γ leads to an improved fit of the segmentation period (Supplementary Information, Figure S3), and a perturbation analysis suggest that this parameter has little effect on somite size and PSM length (Supplementary Information, Figure S4). Using this formulation, we then were able to keep all parameters fixed while only the tail bud growth rate changes during the segmentation process.

We next used the inferred tail bud growth rate as an input to our model and determined the set of parameters that yield the best fit of the model to the PSM length and somite size measured experimentally (Tam 1981). We obtained a good quantitative fit for both experimental conditions (Figures 2C-F). However, we observed that the difference in the growth rate between WT and MMC-treated embryos alone is not enough to explain the differences in somite size and PSM length between these two conditions, and that the characteristic time scale of the amplitude gradient (α) is the parameter that changes the most between these conditions (Figure 2G).

These results suggest that our framework is able to quantitatively reproduce mouse segmentation *in vivo* and that modulations in the growth rate additionally affect the characteristic time scale of the amplitude gradient, suggesting a link between the growth rate and the properties of the cellular oscillators, which is likely to be modulated by Fgf/Wnt signaling.

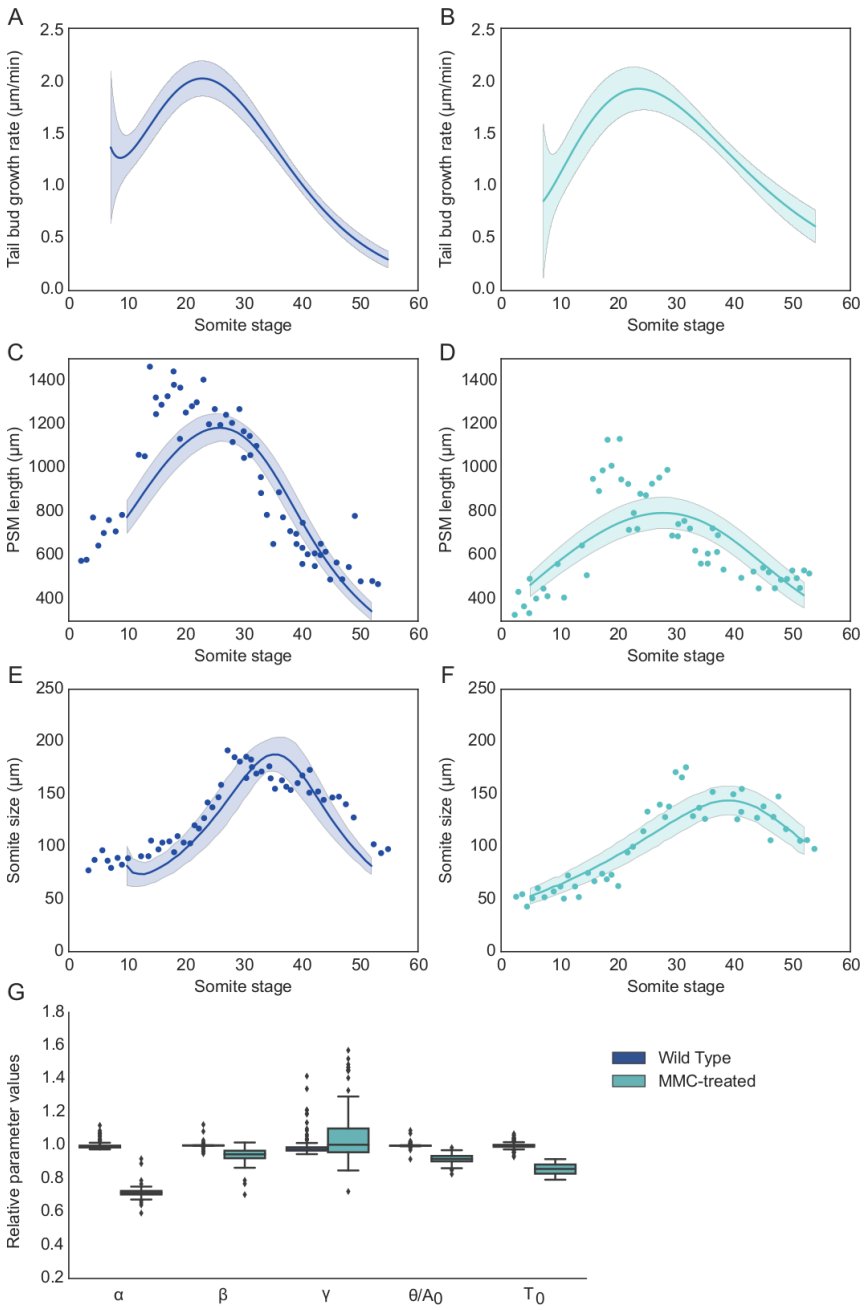

Figure 2. Properties of mouse segmentation in WT and MMC-treated embryos. *A) Inferred tail bud growth rate for different somite stages of WT and B) MMC-treated embryos. Tail bud growth rates were inferred from experimental data (Tam 1981, Figure S1). Lines represent the average fit of a bootstrap resampling and the area represents the 95% confidence interval. C) PSM length for different somite stages for WT and D) MMC-treated embryos. E) Somite size for different somite stages for WT and F) MMC-treated embryos. C-F) Dots represent data from (Tam 1981), lines represent the average fit and the area represents the 95% confidence interval of the model prediction. A total of 100 simulations were evaluated using different fits of the tail bud growth rate, obtained via bootstrap, as an input. G) Comparison of parameter values that best fit the data for WT and MMC-treated embryos. Values are normalized by the average values of WT embryos, which are presented in Table 1.*

Somite size is temperature compensated and controlled by tail bud growth rate and clock period.

In the previous section, we observed that our framework is able to reproduce data from *in vivo* mouse segmentation. In order to gain a better understanding of the properties of our model, we considered a simplified case where the tail bud growth rate is constant (g). This leads to a stationary state where the PSM length and somite size does not change during the segmentation process (Figure 3A,B). We then performed a perturbation on the values of each parameter to identify the key parameters. We observed that PSM length, somite size and segmentation period are controlled mostly by three key parameters: the tail bud growth rate (g), the oscillation period at the tail bud (T_0), and the characteristic length of the amplitude gradient (α). We found that g positively regulates both PSM length and somite size, T_0 positively regulates both the somite size and segmentation period, and α positively regulates the PSM length (Figure 3C). Note that although the amplitude is critical in our model, the phase of the cells during segmentation remains the same for every formed somite (Figure S5). Moreover, posterior cells reach the threshold before the anterior cells in the newly forming somite and the anterior part of the new somite experience high levels of the oscillatory protein (Figure S5 and Supplementary movie 1), consistent with experimental observations in zebrafish (Shih et al, 2015).

According to our model, the size of the somite is proportional to the tail bud growth rate and oscillation period (Figure 3C). It is interesting to note that although growth rates and oscillation periods change broadly with the temperature, somite size is the same for embryos grown at different temperatures (Oates et al, 2012). We then asked what conditions in our model lead to temperature compensation, i.e., what is the specific relationship between the growth rates and period of the oscillators that maintains the size of the somite constant. To evaluate that, we simulated the segmentation process for different values of growth rates and oscillation periods at the tail bud (Figure 3D). We found that a decrease in the oscillation period can compensate larger somite sizes due to increased growth rates (Figure 3D). Thus, our model suggests a temperature compensation mechanism of somite size. This mechanism is consistent with experimental observations in zebrafish showing that both the somitogenesis frequency and the growth rate increase with the temperature, without altering the size of the somites (Schröter et al, 2008, Oates et al, 2012).

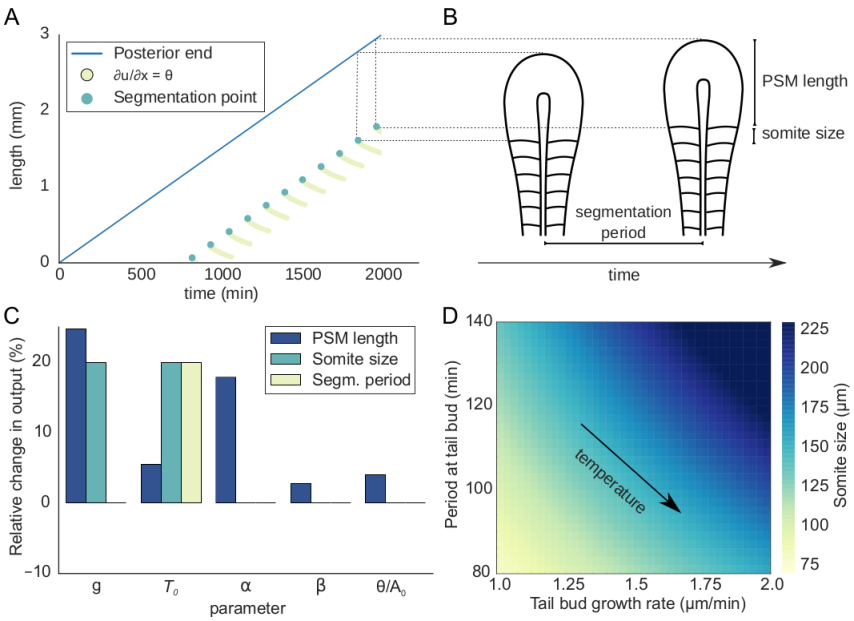

***Figure 3. Segmentation properties at constant tail bud growth rate**. A) Position of posterior end (blue line) and position of segmentation in time. Yellow dots represent the points where $\partial u/\partial x = \theta$ and green dots represent where a new segment is formed. The formation of a new segment happens when $\partial u/\partial x = \theta$ is satisfied in a position x such that x > x_s, where x_s is the position of the previous segment. The phase the cells during segmentation is the same during the whole process (Figure S5). Note that caudal cells reach the threshold before the rostral cells within a somite length. B) Graphical representation of segmentation process. Assuming constant tail bud growth rate, the PSM lengthening is exactly the size of one somite during one segmentation period. C) Parameter sensitive analysis. Each parameter is increased in 20% of its standard value (Table 1). The tail bud growth rate (g), clock period at posterior end (T_0), and the characteristic length of amplitude gradient (α) are the most sensitive parameters, i.e., lead to changes of more than 10% of either PSM length, somite size and segmentation period. PSM length is regulated by both g and α, somite size is regulated by both g and T_0, and segmentation period is controlled by T_0. D) Somite size for different values of T_0 and g. If an increase in g is accompanied by a proportional decrease in T_0, the size of somites remains the same, suggesting a temperature compensation mechanism.*

Somite size is determined at the tail bud.

The size of the somites scale with body size (Cooke 1975) and *ex vivo* explants have shown that segment size scales with mPSM size (Lauschke et al, 2013). Nevertheless, the exact relationship between somite size and PSM length is still unclear and a topic of debate.

In measurements of mouse segmentation (Tam 1981, Figure 2), we observe that the growth rate, PSM length and somite size have a similar profile: an initial increase until reaching a peak to further decrease. Moreover, the peak of the growth rate coincides approximately with

the peak of PSM length, while the peak of the somite size is delayed in relation to growth rate and PSM length (Tam 1981, Figures S1,2). The delayed relationship between the somite size with the PSM length and growth rate is intriguing and suggests that the size of the somites is determined before somite formation. Indeed, it has been suggested that in zebrafish the determination front is defined a few somite stages before segmentation occurs (Akiyama et al, 2014). Moreover, it has been shown that PSM cells in mouse are organized into segmental units before segmentation (Tam 1981).

How early is the segment size defined? Our model assumes a timer mechanism of somite segmentation rather than a positionally controlled segmentation front. Consequently, in our framework, the segment size would be determined as soon as the cells leave the tail bud region. In order to better illustrate this property, we analyzed our model by considering that the tail bud growth rate presents a hump-shaped curve (Figure 4A), similar to what is observed during mouse segmentation (Tam 1981, Figure 2A,B). We observed that the PSM length and somite size profiles also have a shape similar to the growth dynamics (Figure 4B). The peak of PSM length approximately coincides with the peak of the tail bud growth rate, while the peak in segment size is delayed by around 7 somite stages (Figure 4B). It is interesting to note that this delay is approximately the averaged ratio between the PSM length (*P*) and the size of the most recently formed somite (*s*) (Figure 4B). This ratio represents a good estimate of the amount of time, in somite stages, that the cells spend to move from the tail bud until being incorporated into a new somite. Therefore, our model predicts that the difference in the peaks of PSM length and somite size is the amount of time the cells spend to cross the PSM, which is approximately the ratio *P/s*.

The ratio *P/s* vary significantly during development and between different vertebrate species. Mouse and chicken has a ratio of around 7-10, while this ratio is around 10-15 in zebrafish and can vary from 10 to more than 30 in snakes (Gomez et al, 2008). Interestingly, chicken and snakes also present a peak in somite size and PSM length during the segmentation process, while in zebrafish the PSM length decreases during the whole process (Gomez et al, 2008). We then compared the difference in the peaks of somite size and PSM length for mouse, chicken and snakes, and we observed that this difference is approximately the ratio *P/s* (Figure 4C, Gomez et al, 2008).

These results support the idea that the size of the somites depends on the growth rate at the time the cells are at the tail bud. Therefore, according to our model, somite size depends on both the period of oscillation and the tail bud growth rate at the time the cells leave the tail bud region, which can be mathematically represented as:

$$s \approx g_{t0}\, T_0, \tag{14}$$

where g_{t0} is the tail bud growth rate at the time the cells leave the tail bud region ($t = t_0$).

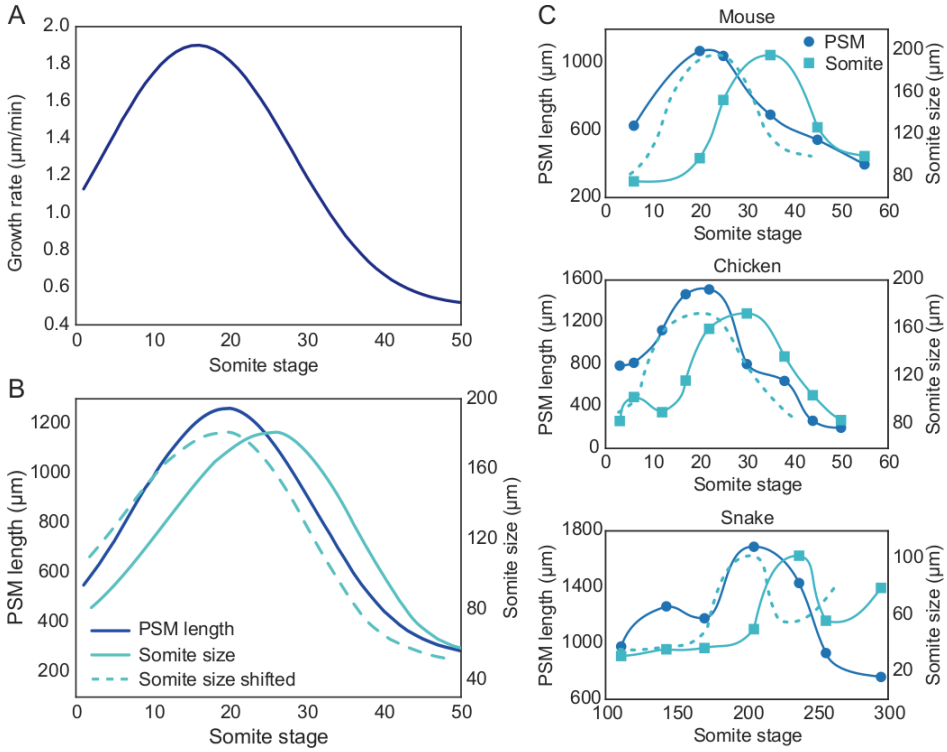

Figure 4. Relationship between tail bud growth rate, somite size and PSM length for dynamic growth rates. *A) Tail bud growth rate for different somite stages. B) Inferred PSM length (blue curve) and somite size (green curve) for the tail bud growth rate presented in A) and with parameters consistent with mouse segmentation (Table 1). The dashed green line represents the somite size curve shifted by the ratio PSM/somite size at the somite stage when PSM length is maximum. C) Experimental measurements of PSM length and somite size during different embryonic stages for mouse, chicken and snake obtained from (Gomez et al, 2008). The dashed curve represents the somite size curve shifted by the ratio PSM/somite size at the somite stage when PSM length is maximum.*

Evolutionary mechanisms of vertebrate segmentation.

There is a large diversity in somite size, number and frequency among vertebrate species, but little is known about the evolutionary mechanisms that lead to such diversity (Gomez et al, 2009). For example, while mouse and chicken share similar segmentation properties, snakes and zebrafish have somites three to four times smaller (Figure 5A). Interestingly, snakes and zebrafish achieve smaller somites via different mechanisms. In zebrafish, smaller somites are mostly due to a decrease in the period of oscillations, while snakes have smaller somites due to slower growth rates (Gomez et al, 2008; Figure 5A). This suggests that differences in the growth rate and period of oscillations are the main evolutionary mechanism to achieve somites with different sizes. But are the changes in these parameters sufficient to explain segmentation properties of these different species? To answer that, we used our model to estimate somite size and PSM length for different values of growth rate and oscillation period

in the tail bud. We found that changes in these parameters alone are sufficient to explain somite size, but not the observed PSM length (Figure S6).

We further asked if concomitant changes in the characteristic length of the gradients (α and β) could explain changes in both somite size and PSM length. Experimental measurements have shown that the increase in the period from posterior to anterior scales with PSM length in a similar fashion between snakes and zebrafish (Gomez et al, 2008). This suggests that the slowing down of the oscillations from posterior to anterior is similar between different species. Therefore, we expect that the ratio between the period at anterior and posterior part of the PSM to be similar for different species, such that:

$$\left(\frac{T_{ant}}{T_0}\right)_{specie_1} = \left(\frac{T_{ant}}{T_0}\right)_{specie_2}. \tag{15}$$

Consequently:

$$\left(e^{-\frac{\tau}{\beta}}\right)_{specie_1} = \left(e^{-\frac{\tau}{\beta}}\right)_{specie_2}, \tag{16}$$

which leads to:

$$\frac{\beta_1}{\beta_2} = \frac{\tau_1}{\tau_2}. \tag{17}$$

Therefore the ratio between the characteristic time scale of the period gradient (β) in different species is proportional to the ratio between the amount of time the cells take to cross the PSM (τ). This amount of time is proportional to the ratio between PSM length and somite size, and can be estimated as:

$$\tau \approx \frac{P}{s}\, T_0. \tag{18}$$

It is interesting to note that both zebrafish and snakes present a higher PSM/somite (P/s) ratio than mouse and chicken. Moreover, this ratio correlates with changes in the tail bud growth rate (*g*), therefore suggesting a possible link between the growth rates and the ratio PSM/somite size (Figure 5B). Using data from different species, we inferred the following relationship between *P/s* and *g* (Figure 5B):

$$\frac{P}{s} \sim g^{-1.5}. \tag{19}$$

.

Taken together, we can estimate the inter-species ratio of the characteristic length of the period as a function of changes in the growth rate and period at the tail bud:

$$\frac{\beta_1}{\beta_2} = \frac{(g^{-1.5}\, T_0)_1}{(g^{-1.5}\, T_0)_2}. \tag{20}$$

Assuming that the inter-species ratio of the characteristic length of the amplitude follows the same relationship, we have:

$$\frac{\alpha_1}{\alpha_2} = \frac{(g^{-1.5}\, T_0)_1}{(g^{-1.5}\, T_0)_2}. \tag{21}$$

Note that these inferred relationships couple the properties of the signaling gradients to the growth rate and period of the oscillators. Such coupling has been shown to lead to a segmentation process that can account for PSM shrinking and growth termination (Jörg et al, 2015; Jörg et al, 2016).

Once we have previously inferred the values of α and β from experimental data for the mouse (Figure 2, Table 1), we took this species as a reference to infer these parameters for other species. We then used our model to estimate the somite size and PSM length for different species and observed that our model correctly captures these values for mouse, chicken, snake and zebrafish (Figure 5C-D). We also observed that snakes show a much larger number of stripes of the oscillatory protein in the PSM than zebrafish, mouse and chicken, which is consistent to experimental observations (Figure 5E, Gomez et al, 2009).

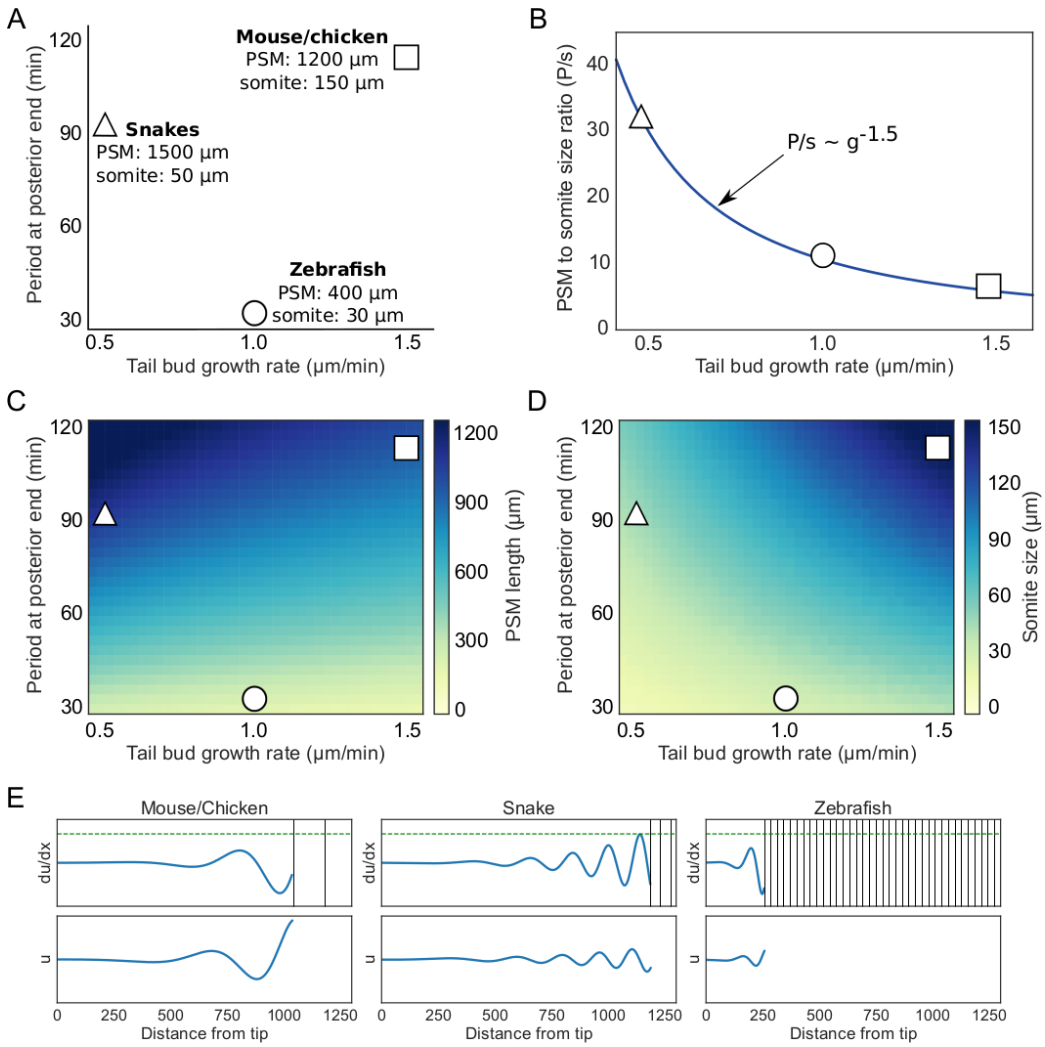

Figure 5. Segmentation properties of different vertebrate species. *A) Representation of the estimated overall growth rate and period in the tail bud, PSM length and somite size for mouse and chicken, snakes and zebrafish (Gomez et al, 2008). B) Relationship between PSM/somite size ratio (P/s) and the tail bud growth rate for different species. Blue line represents the fit that relates the ratio P/s to the growth rate. C) PSM length and D) somite size for different values of growth rate and period at the tail bud. We considered that changes in the growth rate and the period of oscillations also affect the steepness of the gradients. E) Representation of the values of u and* $\partial u/\partial x$ *for different species. Dashed green lines represents the threshold θ, while dark vertical lines represent the position of formed segments.*

Pattern scaling of ex vivo explants with different temperatures.

One interesting property of cells from the PSM is the ability to self-organize into emergent monolayer PSM (mPSM) structures when explanted *in vitro* (Lauschke et al, 2013, Tsiairis and Aulehla 2016). These structures show many properties that resemble *in vivo* segmentation, such as the formation of Fgf/Wnt gradients and patterning, although how the

cells self-organize into such a spatial structure is still unclear (Lauschke et al, 2013, Tsiairis and Aulehla 2016). One of the most interesting properties of these explants is that the segments are formed proportionally to the mPSM size (Lauschke et al, 2013).

During *in vivo* segmentation, the levels of Fgf and Wnt decrease temporally as the cells cross the PSM due to the gradient by inheritance (Dubrulle and Pourquié 2004, Aulehla et al, 2003). In contrast, during *ex vivo* segmentation, the cells have a fixed position in relation to the center of the mPSM and the gradient is formed from center to periphery (Lauschke et al, 2013, Tsiairis and Aulehla 2016). Therefore, *ex vivo* explants offer a good experimental setup to study the behavior of PSM cells when the gradient is spatially formed. To take this into account, we adapted our model by considering that the amplitude and the period gradient change spatially:

$$A = A_0 e^{\frac{\Delta x}{\alpha'}} \tag{22}$$

$$T = T_0 e^{\frac{\Delta x}{\beta'}}, \tag{23}$$

where α' and β' are the characteristic spatial length of the amplitude and period gradients, respectively, and $\Delta x = L - x$, is the distance of the cell x to the center of the mPSM (L). Note that for simplicity we assume a static period gradient, although it has been suggested that the period gradient during *ex vivo* segmentation is dynamic (Lauschke et al, 2013). We reanalyzed the data from (Lauschke et al, 2013) and show that their data is also in agreement with a static period gradient (Supplementary Information, Figures S8,9).

In this case, the position of segmentation can be determined by:

$$A\left[\frac{\omega \Delta t}{\beta'}\cos\phi - \frac{1}{\alpha'}\sin\phi\right] = \theta. \tag{24}$$

We then used this framework to fit the relationship between somite size and wave velocity with PSM length for explants at different temperatures (Figure 6A-D, Lauschke et al, 2013). We observed that most parameters have a similar value, with the exception of the period of oscillations, which is longer for explants at lower temperature (Figure 6E). This is consistent with experimental measurements showing that explants at lower temperature have a longer overall oscillation period (Figure 6F, Lauschke et al, 2013).

Taken together, these results suggest that our framework is able to reproduce somite formation from both *in vivo* and *ex vivo* data. The critical difference between both cases is that a spatial gradient self-emerge in *ex vivo* explants, leading to a scaling of segment size

with the mPSM, whereas *in vivo*, the tail bud growth controls the delayed scaling between somite size and PSM length.

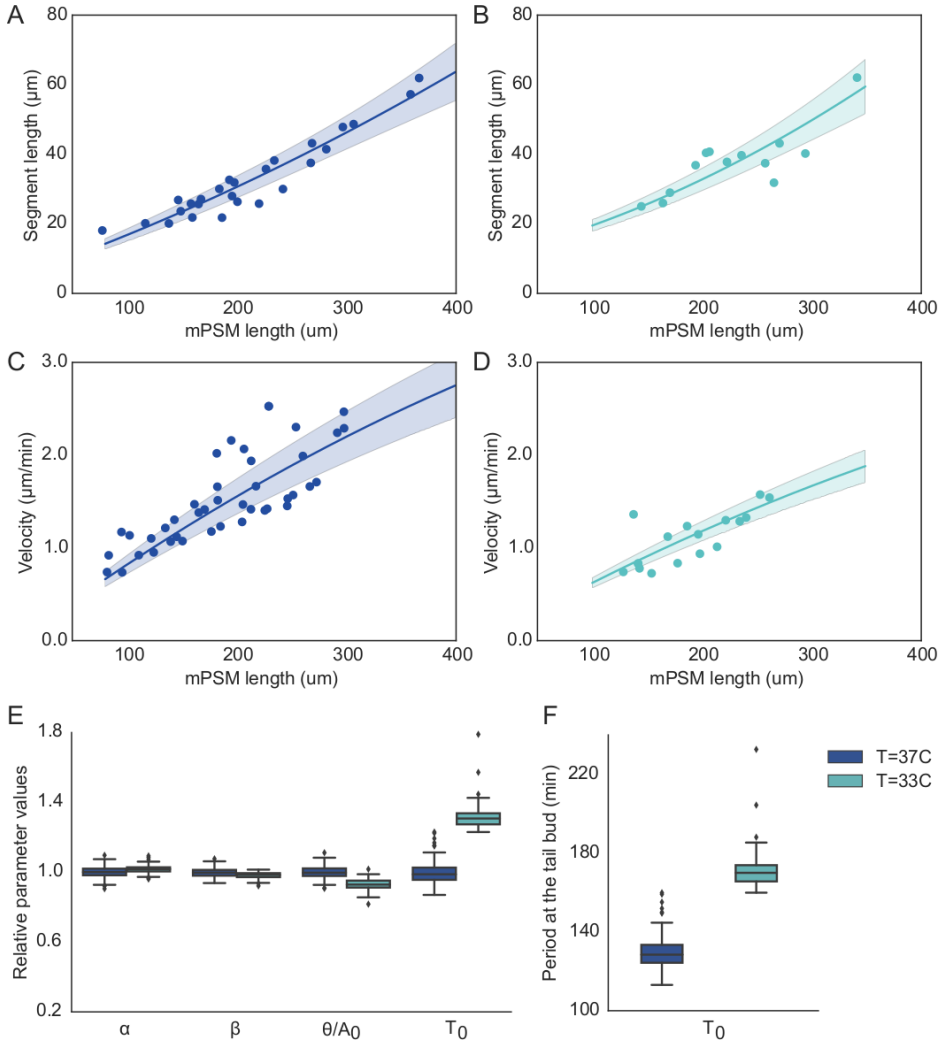

Figure 6. Properties of mouse segmentation in* ex vivo *explants at different temperatures. *A) Segment size and mPSM length for explants at 37°C and B) 33°C. C) Wave velocity and PSM length for explants at 37°C and D) 33°C. The wave velocity is defined by the mPSM divided by the time to form the segment. A-D) Dots represent data from (Lauschke et al, 2013), lines represent the average fit and area represent the 95% confidence interval of the model prediction. E) Comparison of parameter values that best fit the data for explants at temperatures 37°C and 33°C. The values are normalized by the average values of explants at 37°C. Changes in the period at the center of the mPSM (T_0) are required to fit explants from different temperatures. F) The predicted increased period for explants at lower temperatures is consistent with experimental observations of an overall period of 137.4 min and 193.4 min for explants at 37°C and 33°C (Lauschke et al, 2013). Moreover, in order to fit explants at 37°C our model requires a period at the center of the explant of around 130 min, which is consistent with the value obtained experimentally of 132 min (Lauschke et al, 2013).*

Discussion

How the cells obtain their positional information to coordinate somite formation during vertebrate segmentation is an open question in developmental biology. Over the past decades, the "clock-and-wavefront" model has provided an intuitive conceptual framework to understand *in vivo* somite formation and guided much of the experimental research in the field. Among the successes of this model is the prediction that somite size is dependent on the velocity of tail elongation and the period of oscillations. Nevertheless, in this framework, the clock and the wavefront are considered to be two separated entities and recent experiments with *in vitro* PSM cultures have challenge this idea. When transplanted *in vitro*, PSM cells are able to self-organize into a monolayer (mPSM) and present concentric segmentation that scales with the remaining mPSM (Tsiairis and Aulehla, 2016). These results are difficult to interpret with the 'clock-and-wavefront' model and suggest that the segmentation is independent of long-range regulations and is an intrinsic property of the cellular oscillators (Lauschke et al., 2013; Beaupeux and François, 2016). A phase-difference positional information model has successfully explained segmentation in such explants (Lauschke et al., 2013; Beaupeux and François, 2016) and recent experiments have shown that the phase shift between Notch and Wnt signaling can control segmentation in *ex vivo* explants (Sonnen et al, 2018). Nevertheless, the interpretation of *in vivo* segmentation within this framework is not straightforward.

Here, we propose an alternative approach where somite formation is based on local differences in the levels of neighboring cellular oscillators and that the cells use this relative difference as their positional information. Using this framework, we obtain a good quantitative fit of *in vivo* mouse segmentation in both WT and growth disturbed animals, and *ex vivo* explants at different temperatures. Our model has a relatively simple mathematical formulation with few intuitive parameters that can be measured experimentally. Only three parameters control most of the segmentation properties: the tail bud growth rate, the period of oscillations and the characteristic time scale of the amplitude gradient. In the stationary state, the predictions of our model regarding the regulation of somite size are consistent with the "clock-and-wavefront" mechanism. Somite size is regulated by the tail bud elongation rate (wavefront velocity) and the period of the oscillations, and a concomitant modulation of these parameters due to temperature changes leads to the maintenance of same somite size. Nevertheless, our model differs from the "clock-and-wavefront" model regarding the regulation of PSM length. According to the "clock-and-wavefront" model, the length of the PSM is defined by the signaling wavefront, while in our model the PSM length is mostly dependent on the tail bud growth rate. This is a critical difference. In the "clock-and-wavefront" the shrinkage of the PSM observed in most species requires a dynamic change in the properties of the signaling wavefront, while in our model the reduction of the PSM length can be explained with reduced growth rates. Data from mouse segmentation supports the close relationship between PSM length and tail bud growth rates, therefore favoring the

interpretation from our model (Tam 1981, Figure 2). Our model also makes different predictions regarding when the size of the somites is determined. According to the 'clock-and-wavefront' model, the size of the somites is determined only after the cells cross the wavefront, while in our model, it is determined when the cells are still at the tail bud. Because the size of the somites is defined much earlier, our model predicts a delayed scaling between PSM length and somite size, where the delay is approximately the ratio PSM/somite size. We show that experimental data from different species is in agreement with this prediction. All together, these results support the idea that the somite segmentation program is a timer mechanism that works independent of any long-range signal such as morphogens.

We lastly used our theoretical framework to analyze possible developmental mechanisms of somite size control. According to our model, the tail bud growth rate and the period of the oscillators control the size of the somite, but changes in these parameters alone are not sufficient to explain the PSM length and somite size of different species. We observed that the ratio PSM/somite size varies significantly between different species and by analyzing data from mouse, chicken, snakes and zebrafish, we observed that this ratio correlates with changes in tail bud growth rate. We further inferred a relationship between the characteristic time scale of the amplitude and period gradients (α and β) with the tail bud growth rate. We observed that lower growth rates lead to increased α and β and using this inferred relationship, we correctly reproduced the overall segmentation properties in different species. Our results suggest that segmentation at low growth rates leads to an increased PSM/somite size ratio. Whether such longer PSM as compared to somite size leads to evolutionary advantages is unclear. One possible explanation is that the low growth rate observed in snakes is a consequence of low metabolic rates (Gomez et al, 2008), which would also lead to slower mRNA degradation, therefore leading to an increased time scale of the amplitude and period gradients. In this case, longer PSM length such as observed in snakes are just a consequence of slower metabolism.

To the best of our knowledge, our model is the first model to conciliate and quantitatively fit data from both *in vivo* and *ex vivo* experiments. Besides that, we propose developmental mechanisms of somite size control, such as the relationship between growth rates, the amplitude and period gradients, and the ratio PSM to somite size (P/s). We predict that P/s is inversely proportional to the tail bud growth rate. It would be interesting to measure these parameters in other species in order to validate such relationship. Moreover, our model is built on 3 key assumptions that have little or no experimental support and can be seen as predictions to be tested. As the cells cross the PSM, the levels of Fgf and Wnt decrease due to mRNA decay (Dubrulle and Pourquié 2004; Aulehla et al, 2003). Concomitantly, the period and amplitude of Hes/her oscillators increase (Delaune et al, 2012; Shih et al, 2015). Our first assumption is that the increase in period and amplitude of the oscillators is modulated by the temporal decay of Fgf/Wnt gradients. This is a key assumption of our model, as it suggests

that the behavior of the oscillators is independent of any spatial information and only time-dependent. Experimental evidences have shown that Wnt, but not Fgf signaling, modulates the period of Hes/her oscillations in PSM cells (Gibb et al, 2009; Wiedermann et al, 2015; Dubrulle et al, 2001, Sawada et al, 2001). Whether Wnt also modulates the amplitude of the oscillators remains to be confirmed. Second, we assume that the tail bud growth rate is dependent on the levels of Fgf/Wnt at the tail bud, therefore linking the tail bud growth rate with the properties of the oscillators. This suggests the levels of Fgf/Wnt would have a similar dynamic as the growth rates. Recent experiments have shown that both Fgf and Wnt modulates growth at the tail bud (Amin et al, 2016), but an experimental comparison of the levels of Fgf/Wnt at different embryonic stages is still missing. Third, we assume the existence of a molecular mechanism that enables neighboring cells to compare their protein concentration to obtain their positional information. The PSM cells are known to communicate with their neighbors via Notch signaling. Such communication between neighboring cells has been shown to maintain their oscillations synchronized (Riedel-Kruse et al., 2007; Delaune et al., 2012; Jiang et al, 2000) and Notch signaling has been shown to control *Mesp2,* which is required to initiate somite segmentation (Takahashi et al, 2000; Morimoto et al, 2005; Yasuhiko *et al.* 2006). Notch is a versatile signaling pathway (Andersson et al, 2011), but how the cells could use this pathway to both keep their synchronization and read their positional information is unclear. Moreover, recent experiments in zebrafish show that the spatial difference in Fgf signaling output at the determination front is constant during the segmentation process (Simzek and Özbudak, 2018). This suggests that the position of the determination front is determined by the spatial differential levels in Fgf signaling activity (Simzek and Özbudak, 2018). In mice, Fgf signaling activity is dynamic and have been shown to be dependent on Notch activity via *Hes7* expression (Niwa et al, 2011). It is possible that Fgf and Notch work together to form a decoding mechanism of spatial differences in signaling activity between neighboring cells. The molecular mechanisms underlying such a decoder mechanism require further theoretical and experimental investigation.

In summary, we propose a novel mechanism of spatial pattern formation based on the local differences between neighboring oscillators. In our framework, slightly different properties of neighboring oscillators lead to the temporal accumulation of differences in their levels, resulting in travelling waves as observed in a pendulum wave experiment. During vertebrate body segmentation, as the cells flow across the PSM, the oscillations of Hes/her proteins temporally increase in amplitude and period, leading to the accumulation of differences with their neighbors. We propose that the cells use this difference to decode their positional information. It is important to note that this temporal mechanism is different from most patterning mechanism that assume long-range interactions such as morphogen gradients. In our framework, the program of somite formation is already encrypted into the cells before they leave the tail bud region. After that, the cells only need to compare their clock with their neighbor's clock to decide when it is time to form a new segment.

Material and methods

Parameter values

Table1. Parameter values used in the simulations, unless indicated otherwise.

Parameters	Figure 2	Figure 3,4,5	Figure 6
α or α'	145 min	160 min	240 μm
β or β'	1150 min	1200 min	2470 μm
g	from data	1.5 μm/min	------
T_0	81 min	100 min	130 min
ϑ/A_0	1.0	1.0	0.05
ϒ	32 min	30 min	------

Experimental data

Experimental data was obtained from previous published manuscripts. Data from *in vivo* mouse segmentation was obtained from (Tam 1981), *ex vivo* explants from (Lauschke et al, 2013) and different species from (Gomez et al, 2008). Data were extracted from original manuscripts using WebPlotDigitizer 4.1 online tool (https://apps.automeris.io/wpd/).

Code availability

The simulations were evaluated in Python and all source codes are presented as Jupyter notebooks (http://jupyter.org/) for easy visualization and are freely available on: https://git.bsse.ethz.ch/iber/Publications/2018Boareto_AmplitudeModelSomitogenesis

References

Akiyama, R., Masuda, M., Tsuge, S., Bessho, Y. and Matsui, T., 2014. An anterior limit of FGF/Erk signal activity marks the earliest future somite boundary in zebrafish. *Development*, *141*(5), pp.1104-1109.

Amin, S., Neijts, R., Simmini, S., van Rooijen, C., Tan, S.C., Kester, L., van Oudenaarden, A., Creyghton, M.P. and Deschamps, J., 2016. Cdx and T brachyury co-activate growth signaling in the embryonic axial progenitor niche. *Cell reports*, *17*(12), pp.3165-3177.

Andersson, E.R., Sandberg, R. and Lendahl, U., 2011. Notch signaling: simplicity in design, versatility in function. *Development*, *138*(17), pp.3593-3612.

Aulehla, A., Wehrle, C., Brand-Saberi, B., Kemler, R., Gossler, A., Kanzler, B. and Herrmann, B.G., 2003. Wnt3a plays a major role in the segmentation clock controlling somitogenesis. *Developmental cell*, *4*(3), pp.395-406.

Bajard, L., Morelli, L.G., Ares, S., Pécréaux, J., Jülicher, F. and Oates, A.C., 2014. Wnt-regulated dynamics of positional information in zebrafish somitogenesis. *Development*, 141(6), pp.1381-1391.

Beaupeux, M. and François, P., 2016. Positional information from oscillatory phase shifts: insights from in silico evolution. Physical biology, 13(3), p.036009.

Berg, R.E., 1991. Pendulum waves: A demonstration of wave motion using pendula. Am. J. Phys, 59(2), pp.186-187.

Bessho, Y., Sakata, R., Komatsu, S., Shiota, K., Yamada, S. and Kageyama, R., 2001. Dynamic expression and essential functions of Hes7 in somite segmentation. *Genes & development*, *15*(20), pp.2642-2647.

Cooke, J., 1975. Control of somite number during morphogenesis of a vertebrate, Xenopus laevis. *Nature*, *254*(5497), p.196.

Cooke, J. and Zeeman, E. C. 1976. A clock and wavefront model for control of the number of repeated structures during animal morphogenesis. *J. Theor. Biol.* **58**, 455–476.

Delaune, E. A., François, P., Shih, N. P. and Amacher, S. L. (2012). Single-cell-resolution imaging of the impact of Notch signaling and mitosis on segmentation clock dynamics. Dev. Cell 23, 995-1005.

Dequéant, M.L., Glynn, E., Gaudenz, K., Wahl, M., Chen, J., Mushegian, A. and Pourquié, O., 2006. A complex oscillating network of signaling genes underlies the mouse segmentation clock. *science*, *314*(5805), pp.1595-1598.

Dubrulle, J. and Pourquié, O., 2004. fgf8 mRNA decay establishes a gradient that couples axial elongation to patterning in the vertebrate embryo. *Nature*, *427*(6973), p.419.

Dubrulle, J., McGrew, M. J. and Pourquie, O. 2001. FGF signaling controls somite boundary position and regulates segmentation clock control of spatiotemporal Hox gene activation. *Cell* **106**, 219–232.

Flaten, J.A. and Parendo, K.A., 2001. Pendulum waves: A lesson in aliasing. American Journal of Physics, 69(7), pp.778-782.

Forsberg, H., Crozet, F. and Brown, N.A., 1998. Waves of mouse Lunatic fringe expression, in four-hour cycles at two-hour intervals, precede somite boundary formation. *Current biology*, *8*(18), pp.1027-1030.

Gibb, S., Zagorska, A., Melton, K., Tenin, G., Vacca, I., Trainor, P., Maroto, M. and Dale, J.K., 2009. Interfering with Wnt signalling alters the periodicity of the segmentation clock. *Developmental biology*, 330(1), pp.21-31.

Giudicelli, F., Özbudak, E.M., Wright, G.J. and Lewis, J., 2007. Setting the tempo in development: an investigation of the zebrafish somite clock mechanism. *PLoS biology*, 5(6), p.e150.

Gomez, C., Özbudak, E.M., Wunderlich, J., Baumann, D., Lewis, J. and Pourquié, O., 2008. Control of segment number in vertebrate embryos. *Nature*, *454*(7202), pp.335-339.

Gomez, C. and Pourquié, O., 2009. Developmental control of segment numbers in vertebrates. *Journal of Experimental Zoology Part B: Molecular and Developmental Evolution*, *312*(6), pp.533-544.

Hirata, H., Yoshiura, S., Ohtsuka, T., Bessho, Y., Harada, T., Yoshikawa, K. and Kageyama, R. (2002). Oscillatory expression of the bHLH factor Hes1 regulated by a negative feedback loop. Science 298, 840-843. doi:10.1126/science.1074560

Jiang, Y.J., Aerne, B.L., Smithers, L., Haddon, C., Ish-Horowicz, D. and Lewis, J., 2000. Notch signalling and the synchronization of the somite segmentation clock. Nature, 408(6811), p.475.

Jörg, D.J., Oates, A.C. and Jülicher, F., 2016. Sequential pattern formation governed by signaling gradients. *Physical biology*, 13(5), p.05LT03.

Jörg, D.J., Morelli, L.G., Soroldoni, D., Oates, A.C. and Jülicher, F., 2015. Continuum theory of gene expression waves during vertebrate segmentation. *New journal of physics*, 17(9), p.093042.

Kageyama, R., Ohtsuka, T. and Kobayashi, T., 2007. The Hes gene family: repressors and oscillators that orchestrate embryogenesis. *Development*, *134*(7), pp.1243-1251.

Kawamura, A., Koshida, S., Hijikata, H., Sakaguchi, T., Kondoh, H. and Takada, S., 2005. Zebrafish hairy/enhancer of split protein links FGF signaling to cyclic gene expression in the periodic segmentation of somites. *Genes & development*, *19*(10), pp.1156-1161.

Krol, A.J., Roellig, D., Dequéant, M.L., Tassy, O., Glynn, E., Hattem, G., Mushegian, A., Oates, A.C. and Pourquié, O., 2011. Evolutionary plasticity of segmentation clock networks. Development, 138(13), pp.2783-2792.

Lauschke, V.M., Tsiairis, C.D., François, P. and Aulehla, A., 2013. Scaling of embryonic patterning based on phase-gradient encoding. *Nature*, *493*(7430), p.101.

Lewis, J., 2003. Autoinhibition with transcriptional delay: a simple mechanism for the zebrafish somitogenesis oscillator. Current Biology, 13(16), pp.1398-1408.

Masamizu, Y., Ohtsuka, T., Takashima, Y., Nagahara, H., Takenaka, Y., Yoshikawa, K., Okamura, H. and Kageyama, R., 2006. Real-time imaging of the somite segmentation clock: revelation of unstable oscillators in the individual presomitic mesoderm cells. *Proceedings of the National Academy of Sciences,* 103(5), pp.1313-1318.

McGrew, M.J., Dale, J.K., Fraboulet, S. and Pourquié, O., 1998. The lunatic fringe gene is a target of the molecular clock linked to somite segmentation in avian embryos. *Current Biology*, *8*(17), pp.979-982.

Morimoto, M., Takahashi, Y., Endo, M. & Saga, Y. 2005. The Mesp2 transcription factor establishes segmental borders by suppressing Notch activity. *Nature* **435**, 354–359.

Naiche, L. A., Holder, N. & Lewandoski, M. 2011. FGF4 and FGF8 comprise the wavefront activity that controls somitogenesis. *Proc. Natl Acad. Sci. USA* **108**, 4018–4023.

Niwa, Y., Masamizu, Y., Liu, T., Nakayama, R., Deng, C.X. and Kageyama, R., 2007. The initiation and propagation of Hes7 oscillation are cooperatively regulated by Fgf and notch signaling in the somite segmentation clock. *Developmental cell*, *13*(2), pp.298-304.

Oates, A.C. and Ho, R.K., 2002. Hairy/E (spl)-related (Her) genes are central components of the segmentation oscillator and display redundancy with the Delta/Notch signaling pathway in the formation of anterior segmental boundaries in the zebrafish. Development, 129(12), pp.2929-2946.

Oates, A.C., Morelli, L.G. and Ares, S., 2012. Patterning embryos with oscillations: structure, function and dynamics of the vertebrate segmentation clock. *Development*, *139*(4), pp.625-639. doi: 10.1242/dev.063735

Palmeirim, I., Henrique, D., Ish-Horowicz, D. and Pourquié, O. (1997). Avian hairy gene expression identifies a molecular clock linked to vertebrate segmentation and somitogenesis. Cell, 91(5), pp.639-648.

Primmett, D.R., Stern, C.D. and Keynes, R.J., 1988. Heat shock causes repeated segmental anomalies in the chick embryo. *Development*, 104(2), pp.331-339.

Riedel-Kruse, I.H., Müller, C. and Oates, A.C., 2007. Synchrony dynamics during initiation, failure, and rescue of the segmentation clock. *Science*, 317(5846), pp.1911-1915.

Roy, M.N., Prince, V.E. and Ho, R.K., 1999. Heat shock produces periodic somitic disturbances in the zebrafish embryo. *Mechanisms of development*, 85(1-2), pp.27-34.

Sawada, A., Shinya, M., Jiang, Y.J., Kawakami, A., Kuroiwa, A. and Takeda, H., 2001. Fgf/MAPK signalling is a crucial positional cue in somite boundary formation. Development, 128(23), pp.4873-4880.

Schröter, C., Herrgen, L., Cardona, A., Brouhard, G.J., Feldman, B. and Oates, A.C., 2008. Dynamics of zebrafish somitogenesis. *Developmental Dynamics*, *237*(3), pp.545-553. DOI: 10.1002/dvdy.21458

Simsek, M.F. and Özbudak, E.M., 2018. Spatial Fold Change of FGF Signaling Encodes Positional Information for Segmental Determination in Zebrafish. *Cell reports*, 24(1), pp.66-78.

Sonnen, K.F., Lauschke, V.M., Uraji, J., Falk, H.J., Petersen, Y., Funk, M.C., Beaupeux, M., François, P., Merten, C.A. and Aulehla, A. (2018). Modulation of Phase Shift between Wnt and Notch Signaling Oscillations Controls Mesoderm Segmentation. Cell, 172(5), pp.1079-1090.

Shih, N. P., François, P., Delaune, E. A. and Amacher, S. L. (2015). Dynamics of the slowing segmentation clock reveal alternating two-segment periodicity. Development 142, 1785-1793.

Takahashi, Y., Koizumi, K.I., Takagi, A., Kitajima, S., Inoue, T., Koseki, H. and Saga, Y., 2000. Mesp2 initiates somite segmentation through the Notch signalling pathway. Nature genetics, 25(4), p.390.

Takke, C. and Campos-Ortega, J.A., 1999. her1, a zebrafish pair-rule like gene, acts downstream of notch signalling to control somite development. *Development*, *126*(13), pp.3005-3014.

Tam, P.P.L., 1981. The control of somitogenesis in mouse embryos. *Development*, *65*(Supplement), pp.103-128.

Tsiairis, C.D. and Aulehla, A., 2016. Self-organization of embryonic genetic oscillators into spatiotemporal wave patterns. *Cell*, *164*(4), pp.656-667.

Yasuhiko, Y. *et al.* 2006. Tbx6-mediated Notch signaling controls somite-specific Mesp2 expression. *Proc. Natl Acad. Sci. USA* **103**, 3651–3656.

Wiedermann, G., Bone, R.A., Silva, J.C., Bjorklund, M., Murray, P.J. and Dale, J.K., 2015. A balance of positive and negative regulators determines the pace of the segmentation clock. eLife, 4.

Wolpert, L., 1969. Positional information and the spatial pattern of cellular differentiation. Journal of theoretical biology, 25(1), pp.1-47.

Supplementary Information

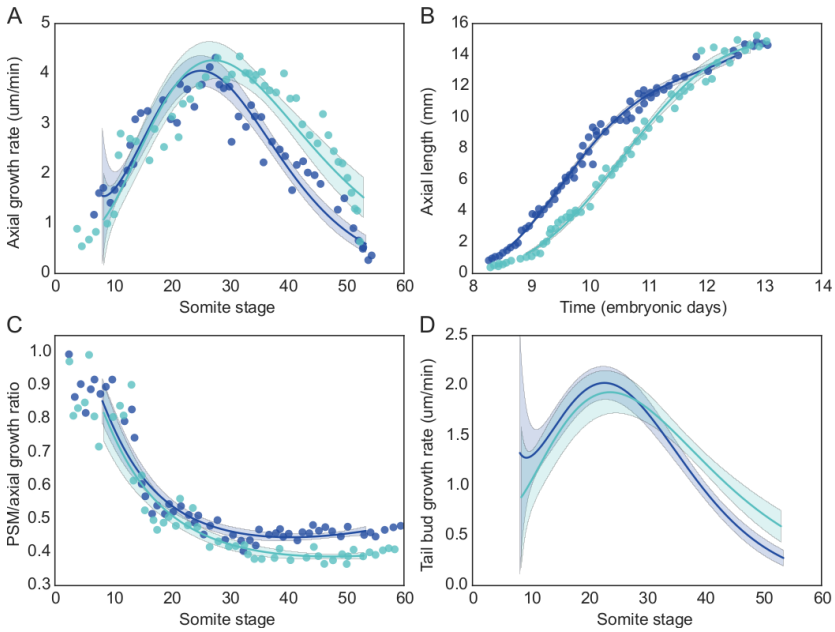

Figure S1. Growth profiles of WT and MMC-treated embryos. *A) Axial growth rate for different somite stages. B) Axial length for different embryonic times. C) Fraction of growth rate due to tail bud elongation for different somite stages. D) Tail bud growth rate for different somite stages inferred by scaling the axial growth rate with the relative growth due to tail bud elongation. A-C) Points represent data from (Tam 1981), solid line represents average fit and*

area represents 95% confidence interval of a bootstrap fit. Dark blue represents WT and light green represents MMC-treated embryos.

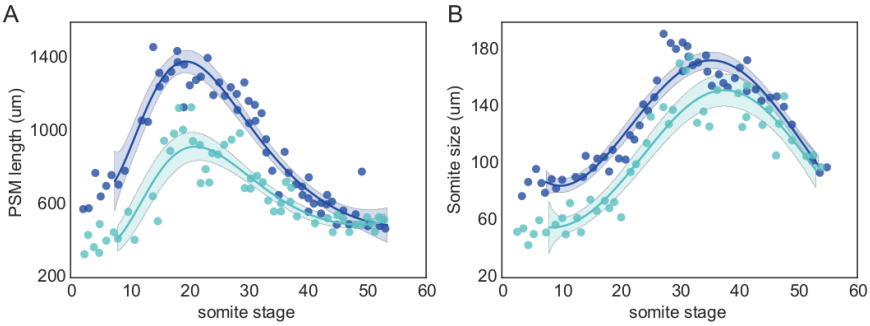

Figure S2. PSM length and somite size profile of WT and MMC-treated embryos. *A) PSM length for different somite stages. B) Somite size for different somite stages. Points represent data from Tam 1981, solid line represents average fit and area represents 95% confidence interval of a bootstrap fit. Dark blue represents WT and light green represents MMC-treated embryos.*

Model formulation considering dynamic period and amplitude at the tail bud.

In order to reproduce *in vivo* data, we considered that the amplitude and period of the oscillations at the tail bud are dependent on tail bud growth rate, such as:

$$A_0 = A'_0 e^{-\frac{g_{t0}}{\gamma}} \tag{S1}$$

$$T_0 = T'_0 e^{-\frac{g_{t0}}{\gamma}}, \tag{S2}$$

where g_{t0} is the growth rate when the cell is at the tail bud (at $t = t_0$), and γ is a constant. Then, the amplitude and period gradient can be expressed as:

$$A = A'_0 e^{-\frac{g_{t0}}{\gamma}} e^{\frac{\Delta t}{\alpha}} \tag{S3}$$

$$T = T'_0 e^{-\frac{g_{t0}}{\gamma}} e^{\frac{\Delta t}{\beta}}, \tag{S4}$$

and segmentation can be estimated by the following equation:

$$\frac{\partial u}{\partial x} = A\left[\left((\omega_0 - \omega)\cos\phi - \frac{1}{\alpha}\sin\phi\right)\frac{1}{g_{t0}} + \left((\omega_0 t_0 + \omega_0\beta - \omega\beta)\cos\phi - \sin\phi\right)\frac{1}{\gamma}\frac{\partial g_{t0}}{\partial x}\right] \quad \text{(S5)}$$

where $\frac{\partial g_{t0}}{\partial x}$ represents the difference in the growth rate at the tail bud region between neighboring cells, which is expected to be small. This leads to the following simplified expression for obtaining the position of segmentation:

$$\frac{A}{g_{t0}}\left[(\omega_0 - \omega)\cos\phi - \frac{1}{\alpha}\sin\phi\right] = \theta. \quad \text{(S6)}$$

We noted that assuming a dynamic modulation of the amplitude and period leads to a better overall fit of experimental data (Figure S3) and that perturbations on the values of γ have a little effect on the PSM length, somite size and segmentation period (Figure S4).

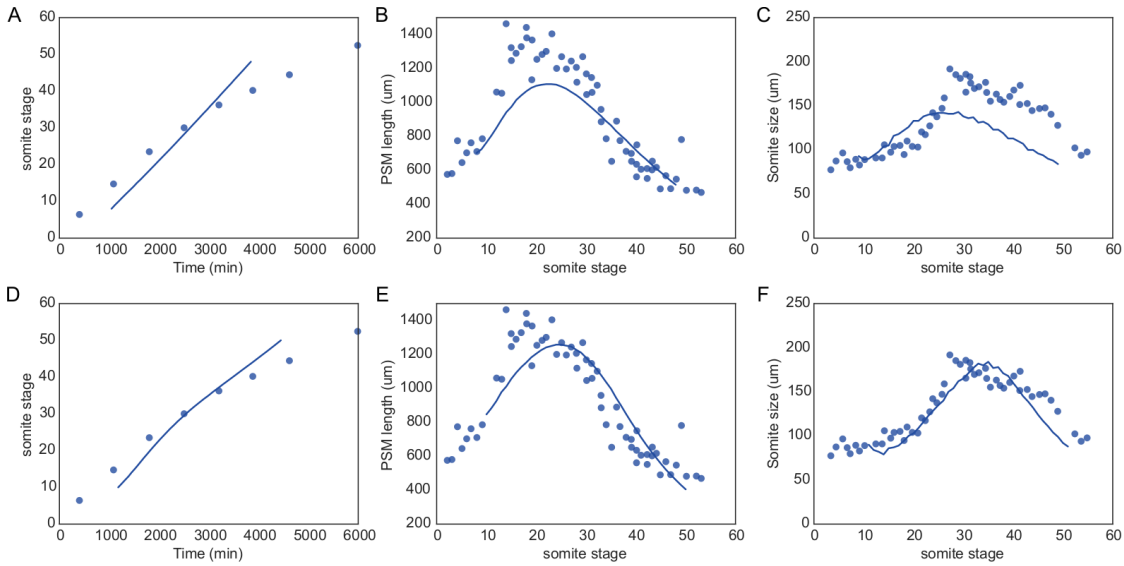

Figure S3. Fit of mouse* in vivo *segmentation data. *A,D) Relationship between somite stage and embryonic time. B-E) PSM length at different somite stages. C,F) Somite size at different somite stages. Circles represent data from (Tam 1981) and lines represent the fit from the modeling using the average value of tail bud growth rate as input. A-C) Modeling results when considering constant period and amplitude at the tail bud. D-F) Modeling results when considering that the period and amplitude at the tail bud are dynamic and dependent on the tail bud growth rate.*

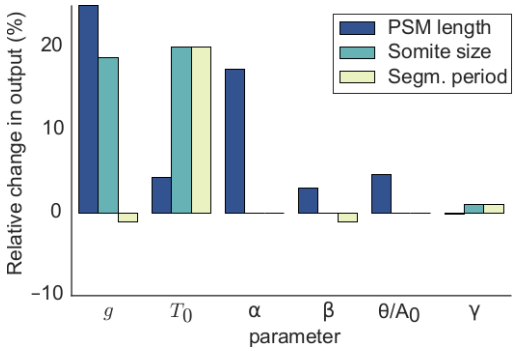

Figure S4. Sensitive analysis by considering the period and amplitude at the tail bud is dependent on the growth rate. *The extra parameter γ has little effect on PSM length, somite size and segmentation period.*

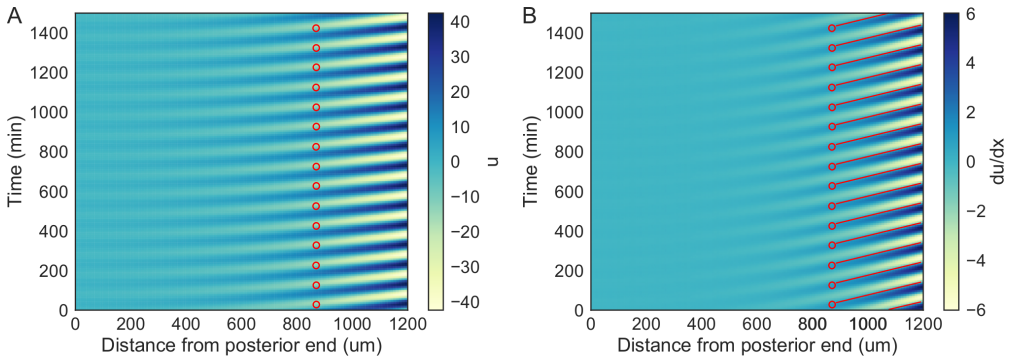

Figure S5. Properties of the oscillators during segmentation. *A) Levels of the oscillators and B) its spatial derivative as a function of time and position related to the posterior end. Red dots and lines represent the position of formation of a new segment, i.e., where du/dx = θ. Note that* the caudal cells reach the threshold before the rostral cells within a somite length. The distance between the previous somite and the first most caudal cell to reach the threshold define the somite size.

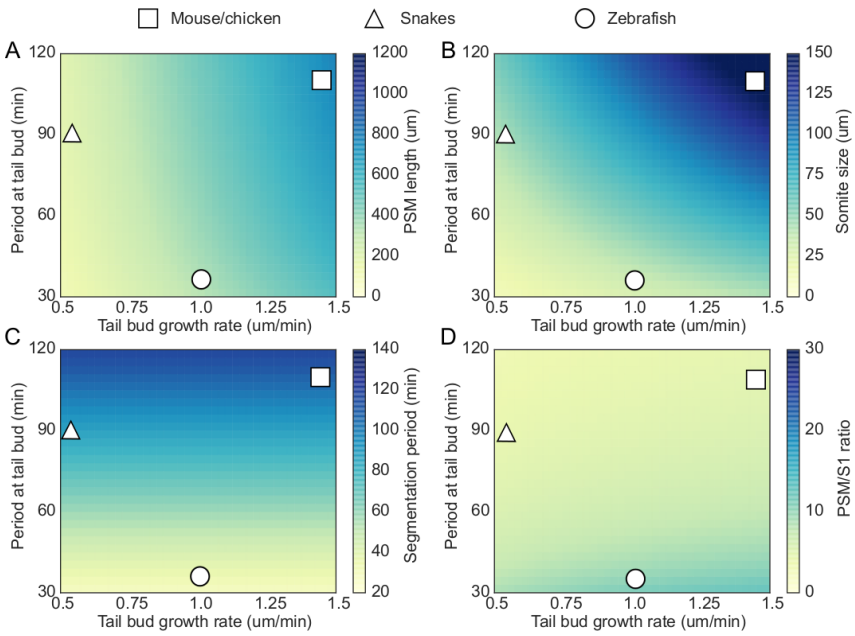

Figure S6. *A) PSM length, B) somite size, C) segmentation period and D) PSM/somite size ratio for different values of growth rate and period at the tail bud. The characteristic length of amplitude and period gradient is remained constant (same values of Figure 3, see Table 1). Note that in this case, our model would predict that snakes would have a much smaller PSM length (around 300 μm). This is in contrast with experimental evidences showing that snakes have a PSM length of around 1200 μm (Gomez et al, 2008).*

Static period gradient in ex vivo explants

In (Lauschke et al, 2013) the authors introduce a new experimental setup to study segment formation in vertebrates. Presomitic mesoderm (PSM) cells are cultured in a dish, forming a monolayer of cells (mPSM) that recapitulates tissue segmentation. Using a Notch reporter, they show that waves of Notch activity propagates from the center to the periphery of the tissue culture, while segmentation occurs from periphery to center, resembling the anterior to posterior segmentation observed *in vivo*. The authors compare the size of the segments with the length of mPSM (the portion of the tissue that remains undifferentiated) and observe that the size of the segment scales with the mPSM length (Figure 3, Lauschke et al, 2013). They also observe a scaling in the velocity of the oscillatory waves of Notch signaling (Figure 3, Lauschke et al, 2013). Using our theoretical framework, we recapitulate both the segment scaling with the mPSM length and the scaling of the velocities of the oscillatory waves of Notch activity (Figure 6).

The authors go on to propose that the observed scaling of the segments with the length of the mPSM arises via a phenomenon that they refer to as period gradient scaling. To this end, the authors show that the phase (ϕ) of oscillations always completes 2π over the unsegmented

domain (mPSM), even though the length of mPSM, L, decreases every time a new segment is formed. Consequently, the slope of the phase gradient ($\frac{\Delta\phi}{\Delta x}$ =2π/*L)* increases in time. Lauschke and co-workers quantified this increase in the phase gradient with time (note that time is linearly related to oscillation number – Figure S7), and showed that it can be described by an exponential function (Figure 4b, Lauschke et al, 2013, which we digitalised and reproduce as Figure S8). The authors went on to show that this exponential relationship would result in the scaling of the period gradient.

In our model, we consider a spatial period gradient that is constant in time. In case of such a static period gradient, the phase (ϕ) and the slope of the phase-gradient ($\frac{d\phi}{dx}$) are linear in time (rather than exponential) and are given by: $\phi = \omega\, t$ and $\frac{d\phi}{dx} = \frac{d\omega}{dx}\, t$, respectively, where $\omega = \omega(x)$ represents the frequency of oscillations.

At first sight, one might think that a linear relationship can be clearly distinguished from an exponential relationship. However, this is only the case if the exponent in the exponential function is sufficiently large and the time period over which the function is observed is sufficiently long. This is not the case for the reported segmentation data: the experimentally determined time-dependency of the phase gradient can be fitted just as well by a linear function (Figure S8, red line), and we confirm that our model recapitulates this relationship just as well (Figure S9, red).

We note that the authors previously showed that the period at the center remains constant during the segmentation process (Lauschke et al, 2013, Figure Supplementary 4). We would argue that in light of this experimental observation, it is actually rather likely that the same applies also to the rest of the domain such that a static frequency gradient would be a better representation of the data.

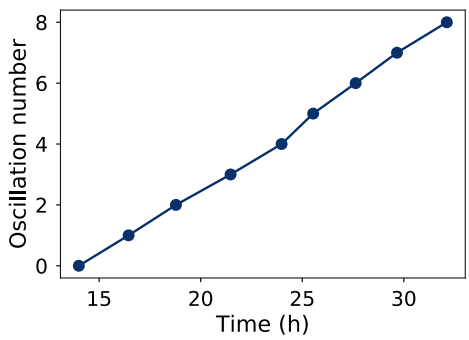

Figure S7. Linear relationship between oscillation number and time. *Blue dots represent the time of formation of a new segment (digitalized from Figure 4a, Lauschke et al, 2013). The slope of the curve represents the time it takes to form a new segment and is approximately the period at the center of the periphery (132 min,* Lauschke et al, 2013, Figure Supplementary 4).

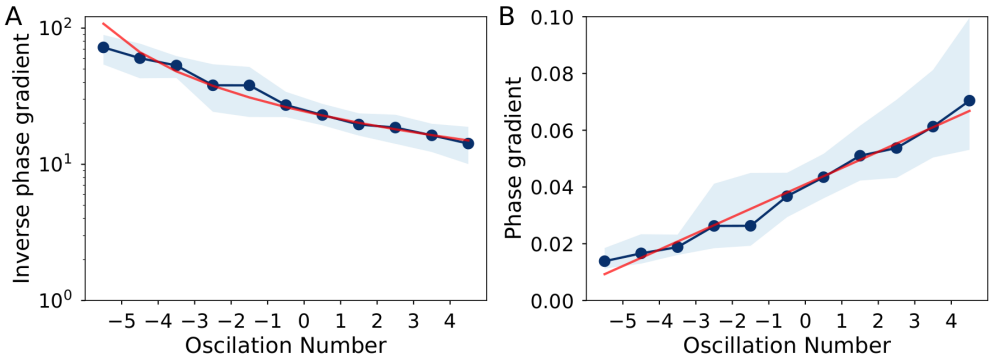

***Figure S8. Linear fit of spatial phase-gradient**. A) Inverse of the spatial phase-gradient as a function of oscillations number, as represented in (Lauschke et al, 2013, Figure 4b). B) Spatial phase-gradient as a function of oscillations number. Blue line represents experimental data and area represents the experimental standard deviation and red line represents a linear fit. Negative oscillation numbers represent a spatial projection of incomplete segmentations (Lauschke et al, 2013).*

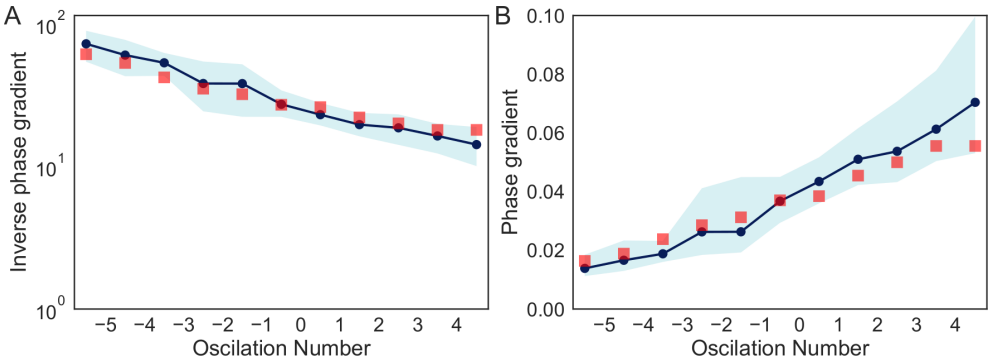

***Figure S9. Spatial phase-gradient in time**. A) Inverse of the spatial phase-gradient as a function of oscillations number, as represented in (Lauschke et al, 2013, Figure 4b). B) Spatial phase-gradient as a function of oscillations number. Blue line represents experimental data and area represents the experimental standard deviation. Red dots represent the relationship obtained by our model.*

Supplementary Movies

Supplementary movie 1. Dynamical representation of the values of u and $\partial u/\partial x$ for different species. Dashed green lines represents the threshold θ, while dark vertical lines represent the position of formed segments.